

## Point load actuation on plate structures based on triangular piezoelectric patches

Gilles Tondreau<sup>\*</sup>, Sudharsana Raamanujan Raman<sup>a</sup> and Arnaud Deraemaeker<sup>b</sup>

*ULB, Building Architecture and Town Planning, 50 av. Franklin Roosevelt, CP 194/02, B-1050  
Brussels, Belgium*

*(Received March 29, 2013, Revised November 20, 2013, Accepted December 13, 2013)*

**Abstract.** This paper investigates the design of a perfect point load actuator based on flat triangular piezoelectric patches. Applying a difference of electric potential between the electrodes of a triangular patch leads to point loads at the tips and distributed moments along the edges of the electrodes. The previously derived analytical expressions of these forces show that they depend on two factors: the width over height ( $b/l$ ) ratio of the triangle, and the ratio of the in-plane piezoelectric properties ( $e_{31}/e_{32}$ ) of the active layer of the piezoelectric patch. In this paper, it is shown that by a proper choice of  $b/l$  and of the piezoelectric properties, the moments can be cancelled, so that if one side of the triangle is clamped, a perfect point load actuation can be achieved. This requires  $e_{31}/e_{32}$  to be negative, which imposes the use of interdigitated electrodes instead of continuous ones. The design of two transducers with interdigitated electrodes for perfect point load actuation on a clamped plate is verified with finite element calculations. The first design is based on a full piezoelectric ceramic patch and shows superior actuation performance than the second design based on a piezocomposite patch with a volume fraction of fibres of 86%. The results show that both designs lead to perfect point load actuation while the use of an isotropic PZT patch with continuous electrodes gives significantly different results.

**Keywords:** shaped piezocomposite actuators; interdigitated electrodes; triangular piezoelectric transducers; point load actuation

### 1. Introduction

Piezoelectric transducers are commonly used in active vibration control (Preumont 2008) and structural health monitoring applications based on impedance measurements (Park 2003). In particular, thin piezoelectric sensors and actuators are used to induce bending vibrations or propagating waves in plate-like structures (Raghavan 2007). Alternatively, they can be used to measure masses down to molecular or atomic levels in the field of biomolecular and chemical detection (Isarakorn 2011), or to actuate special micro-tools in the context of cell manipulation, microsurgery and nanotechnology processes (Carbonari 2009). The main advantages of such transducers are their small size, their high bandwidth and their relatively low price. The most

---

<sup>\*</sup>Corresponding author, Ph. D. Student, E-mail: [gilles.tondreau@ulb.ac.be](mailto:gilles.tondreau@ulb.ac.be)

<sup>a</sup> Ph. D. Student, E-mail: [sraman@ulb.ac.be](mailto:sraman@ulb.ac.be)

<sup>b</sup> FNRS Research Associate, E-mail: [adema@ulb.ac.be](mailto:adema@ulb.ac.be)

common piezoelectric flat transducers are made either of PZT ceramic material (for actuation and/or sensing) or polymer PVDF material (mainly for sensing). Typical piezoelectric transducers found on the market are rectangular or circular. Different researchers have however studied the possibility to use more complex shapes. This idea was mainly driven by the active control applications. The first developments in this direction concern triangular actuators (Burke 1987). Using the theory of distributions and the beam theory, the authors show that applying a voltage  $V$  across the electrodes of the transducer is equivalent to applying two point forces and one bending moment on the supporting structure. If the triangular actuator is clamped, the resulting force is a single point force at the tip of triangle. Coupling this transducer with an accelerometer placed at the tip of the triangle leads to a collocated actuator/sensor pair and the possibility to design a simple and theoretically stable control strategy (Gardonio 2005, 2010, Schiller 2008). The main advantage of the transducer is the very limited mass and volume added to the structure compared to an electrodynamic inertial actuator (Paulitsch 2007).

Shaped transducers have also been used for the design of modal sensors and actuators (Lee 1990a,b, Lee 1991) as an alternative to modal filters obtained from discrete sensor arrays suffering from the spatial aliasing effect (Donoso 2009), and more recently in order to measure the bending moment at the boundary of structures (Chesné 2008). Other research studies suggest that shaped piezoelectric transducers can be used for structural health monitoring (Friswell 2010b) or to harvest vibration energy for powering low energy electronic devices (Friswell 2010a). Recent studies have focused on topology optimization as a tool to find optimal complex shapes of piezoelectric transducers (Lin 2013).

In the studies presented above dealing with triangular patches, the equivalent loads have been computed using the beam theory. In practice however, for many applications involving flat piezoelectric transducers attached to thin plate-like structures, the transverse effects cannot be neglected. In order to correctly compute the equivalent loads, it is therefore necessary to use the plate theory. For triangular actuators, equivalent loads have been computed using Kirchoff's plate theory and the theory of distributions in (Sullivan 1996, 1997), but the expressions derived have been found to be erroneous: the system of forces is not self-equilibrated and symmetry is violated when considering an equilateral triangle with isotropic material properties. In (Deraemaeker 2011), correct expressions have been derived using Hamilton's principle. These expressions show that triangular actuators generate equivalent forces under the form of distributed moments along the edges, as well as point forces at each tip of the triangle which depend on the material properties and the geometry of the triangle. In general, the distributed moments are important, explaining the limited performances of point load actuators designed with triangular PZT ceramic patches and continuous electrodes.

The motivation of this paper is to demonstrate that it is possible to design a real point load actuator based on triangular piezoelectric patches by tailoring its geometry and piezoelectric properties. After recalling the constitutive equations of piezoelectric transducers and summarizing the general form of the equivalent loads applied by a flat piezoelectric actuator, we derive the condition to achieve perfect point load actuation without distributed moments along the edges of the triangular actuator and discuss the practical implementation. The solution consists in using a piezocomposite patch with interdigitated electrodes whose aspect ratio is dependent on the volume fraction of fibers in the piezocomposite layer. Using the commercial finite element package *SAMCEF* (<http://www.samcef.com>), we perform finite element computations using multi-layer plate piezoelectric elements. The results obtained with the triangular patch with interdigitated electrodes are compared with the results obtained with a point force, showing a perfect match.

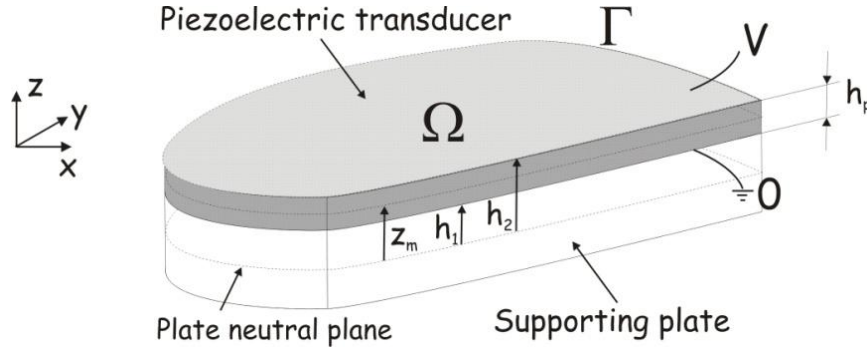


Fig. 1 Two-dimensional piezoelectric transducer attached on a plate

## 2. Derivation of equivalent forces for plate structures

Consider the two-dimensional piezoelectric transducer of thickness  $h_p$  fixed on a plate as illustrated in Fig. 1.

We denote  $\Gamma$  the closed curve bounding the plane region  $\Omega$  on which the transducer is attached.  $x$  and  $y$  are the coordinates along the neutral plane of the plate, not especially coinciding with the principal axis of the piezoelectric material.  $z_m$  is the distance between the mid-plane of the piezoelectric transducer and the neutral plane of the plate. The poling direction is assumed to be in the  $z$  direction, leading to a transverse electric field  $E_3 = -V/h_p$  (assumed to be constant) in the same direction when a voltage  $V$  is applied between the top and the bottom surface electrodes ( $E_1 = E_2 = 0$ ). Assuming plane-stress hypothesis, the out of plane stress components are equal to zero, and using the standard IEEE (Institute of Electrical and Electronics Engineers) notations for linear piezoelectricity, the constitutive equations for the transducer read

$$\begin{pmatrix} T_1 \\ T_2 \\ T_6 \\ D_3 \end{pmatrix} = \begin{pmatrix} c_{11}^E & c_{12}^E & 0 & -e_{31} \\ c_{21}^E & c_{22}^E & 0 & -e_{32} \\ 0 & 0 & c_{66}^E & 0 \\ e_{31} & e_{32} & 0 & \varepsilon_{33}^S \end{pmatrix} \begin{pmatrix} S_1 \\ S_2 \\ S_6 \\ E_3 \end{pmatrix}, \quad (1)$$

where  $E_i$  and  $D_i$  are the components of the electric field and the electric displacement vectors, while  $T_i$  and  $S_i$  are the components of the stress and strain vectors.  $e_{ij}$  and  $\varepsilon_{33}$  are the piezoelectric and dielectric constants respectively. The superscripts indicate whether the properties are measured under constant electric field ( $E$ ) or constant strain ( $S$ ). The constitutive equations can also be written in the matrix form of Eq. (2) if the piezoelectric transducer's material axes make an angle  $\theta$  with the structural axis as illustrated in Fig. 2.

$$\begin{aligned} \{T\}_{xy} &= [c^{E*}] \{S\}_{xy} - [e^*] \{E\} \\ \{D\} &= [e^*]^T \{S\}_{xy} - [\varepsilon^S] \{E\} \end{aligned} \quad (2)$$

where  $[c^{E*}]$  is the stiffness matrix expressed in structural axis  $(x, y)$ , and

$$[e^*] = \begin{bmatrix} e_{31}^* \\ e_{32}^* \\ e_{36}^* \end{bmatrix} \quad (3)$$

with

$$\begin{aligned} e_{31}^* &= e_{31} \cos \vartheta + e_{32} \sin \vartheta \\ e_{32}^* &= e_{31} \sin \vartheta + e_{32} \cos \vartheta \\ e_{36}^* &= (e_{31} - e_{32}) \cos \theta \sin \theta \end{aligned} \quad (4)$$

In (Deraemaeker 2011), the authors show that using the Kirchoff's plate theory and invoking Hamilton's principle, the equivalent distributed loads applied to the supporting plate due to a voltage  $V$  applied between the electrodes are  $(e_{31}^*, e_{32}^*, e_{36}^*, z_m$  and  $V$  are supposed constant):

$$\begin{aligned} p &= 0 \\ M_{nn} &= -e_{31}^* n_x^2 z_m V - e_{32}^* n_y^2 z_m V - 2e_{36}^* n_x n_y z_m \\ -\frac{\partial M_{nt}}{\partial s} + t_{nz} &= -(e_{32}^* - e_{31}^*) z_m V \frac{\partial (n_x n_y)}{\partial s} - 2e_{36}^* z_m V \frac{\partial (n_x^2)}{\partial s} \\ &\quad - \left( (e_{32}^* - e_{31}^*) [n_x n_y] + 2e_{36}^* [n_x^2] \right) z_m V, \end{aligned}$$

where  $p$  is the pressure acting on the plate,  $M_{nn}$ ,  $M_{nt}$ , and  $t_{nz}$ , are the distributed bending moment, torsional moment and shear forces acting on the contour of the patch (Fig. 3).  $(n_x, n_y)$  is the normal external to the contour  $\Omega$ , and  $[.]$  denotes the discontinuity jump. It can be seen that the equivalent loads depend on the piezoelectric coefficients as well as on the analytical expression of the normal to the contour of the piezoelectric patch. In particular, the second line of the last equation of Eq.(5) shows that a discontinuity in the orientation of the normal  $(n_x, n_y)$  will create point forces if  $e_{31}^* \neq e_{32}^*$  (orthotropic piezoelectric material).

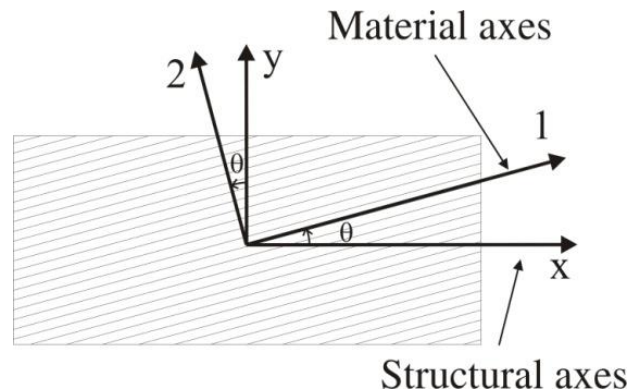


Fig. 2 Orientation of the material axes (1,2) with respect to the structural axes  $(x, y)$

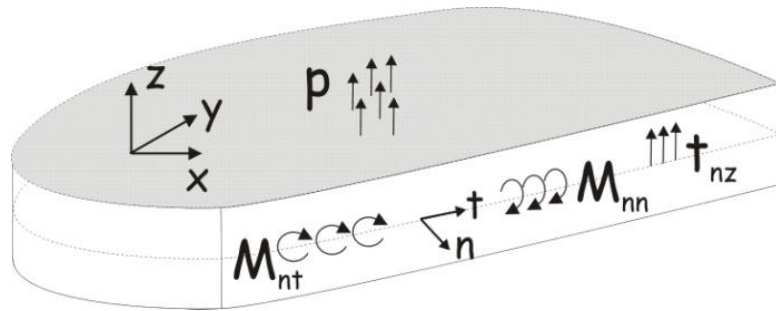


Fig. 3 Distributed external forces acting on the plate

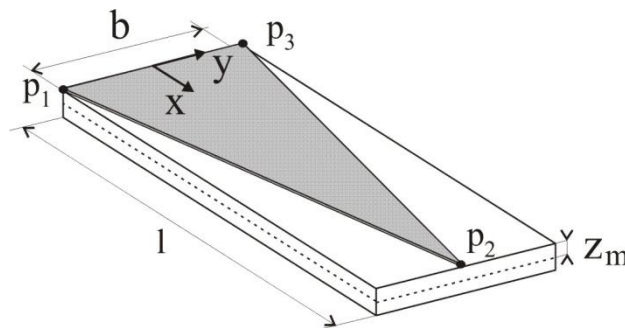


Fig. 4 Triangular actuator aligned with the structural axis

### 3. Design of a point load actuator based on a triangular piezoelectric patch

#### 3.1 Equivalent loads for a triangular piezoelectric actuator

Let us assume a triangular piezoelectric transducer as depicted in Fig. 4, for which the material axes are aligned with the structural axes ( $e_{36}^* = 0$ ):

The distributed loads acting on the contour of the electrodes are given by

$$\begin{aligned}
 -\frac{\partial M_{nt}}{\partial s} + t_{nz} &= -(e_{32} - e_{31})[n_x n_y] z_m V \\
 M_{nn} &= (-e_{31} n_x^2 - e_{32} n_y^2) z_m V
 \end{aligned}
 \tag{6}$$

If the vertices of the triangle are placed at points  $p_1 = (0, -b/2)$ ,  $p_2 = (l, -0)$  and  $p_3 = (0, b/2)$ , the normal vector reads

$$n = \begin{cases} (-1, 0) & \text{on the edge } p_1 p_3 \\ \frac{1}{\sqrt{\frac{b^2}{4} + l^2}} \left( \frac{b}{2}, -l \right) & \text{on the edge } p_1 p_2 \\ \frac{1}{\sqrt{\frac{b^2}{4} + l^2}} \left( \frac{b}{2}, l \right) & \text{on the edge } p_2 p_3 \end{cases}
 \tag{7}$$

This leads to the equivalent loads of Eqs. (8) and (9), which are represented in Fig. 5

$$-\frac{\partial M_{nt}}{\partial s} + t_{nz} = \begin{cases} (e_{32} - e_{31}) \frac{bl}{2(\frac{b^2}{4} + l^2)} z_m V & \text{at point } p_1 \\ -(e_{32} - e_{31}) \frac{bl}{\frac{b^2}{4} + l^2} z_m V & \text{at point } p_2 \\ (e_{32} - e_{31}) \frac{bl}{2(\frac{b^2}{4} + l^2)} z_m V & \text{at point } p_3 \end{cases} \quad (8)$$

$$M_{nn} = \begin{cases} -e_{31} z_m V & \text{on the edge } p_1 p_3 \\ -\frac{\frac{b^2}{4} e_{31} + l^2 e_{32}}{\frac{b^2}{4} + l^2} z_m V & \text{on the edge } p_1 p_2 \\ -\frac{\frac{b^2}{4} e_{31} + l^2 e_{32}}{\frac{b^2}{4} + l^2} z_m V & \text{on the edge } p_2 p_3 \end{cases} \quad (9)$$

In particular, it can be observed that there are no point forces and that the distributed moments are  $M_1 = M_2 = -e_{31} z_m V$  for an isotropic triangle ( $e_{31} = e_{32}$ ), whatever the dimensions of the triangle are.

In order to design a perfect point load actuator, one has to cancel the distributed moment  $M_2$ , which links the geometry of the transducer to the piezoelectric constants  $e_{31}$  and  $e_{32}$ , as stated in Eq. (10)

$$M_2 = -\frac{\frac{b^2}{4} e_{31} + l^2 e_{32}}{\frac{b^2}{4} + l^2} z_m V = 0 \rightarrow \frac{b}{l} = 2 \sqrt{\frac{-e_{32}}{e_{31}}} \quad (10)$$

The corresponding point load reads

$$P = -e_{31} \frac{b}{l} z_m V \quad (11)$$

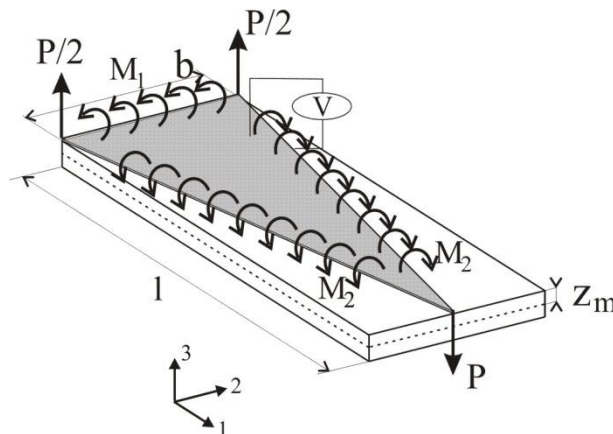


Fig. 5 Equivalent loads for a triangular piezoelectric actuator

The condition of Eq. (10) to cancel the distributed moment  $M_2$  can only be satisfied if the piezoelectric coefficients have opposite signs, which is not the case with the piezoelectric transducers poled through the thickness. In order to solve this issue, poling in one of the directions of the plane of the actuator should be performed, which requires the use of interdigitated electrodes. In addition, Eq. (10) shows that the shape of the triangle is linked to the ratio of the in-plane piezoelectric properties. By modifying this ratio, the shape of the triangle can therefore be adapted. The next section discusses the use of piezocomposite transducers which allow varying the  $e_{31}/e_{32}$  ratio, as already addressed by the authors of this paper in (Raman 2012). Note that a similar approach was followed in (Schiller 2008), based on the erroneous equations of (Sullivan 1997). The authors found the same condition to cancel the moments, but the corresponding point load was not correct.

### 3.2 Piezocomposite transducers

To overcome the major drawbacks of the PZT ceramics (brittleness and very low flexibility), piezocomposite transducers (Newnham 1980, Williams 2002) in which piezoelectric fibers are mixed with a softer passive epoxy matrix have been developed. One of the most successful realizations of such transducers is the Macro Fiber Composite (MFC) transducers manufactured and sold by the company *Smart Material*. The transducers are made of an active layer sandwiched between two soft encapsulating layers (Fig. 6).

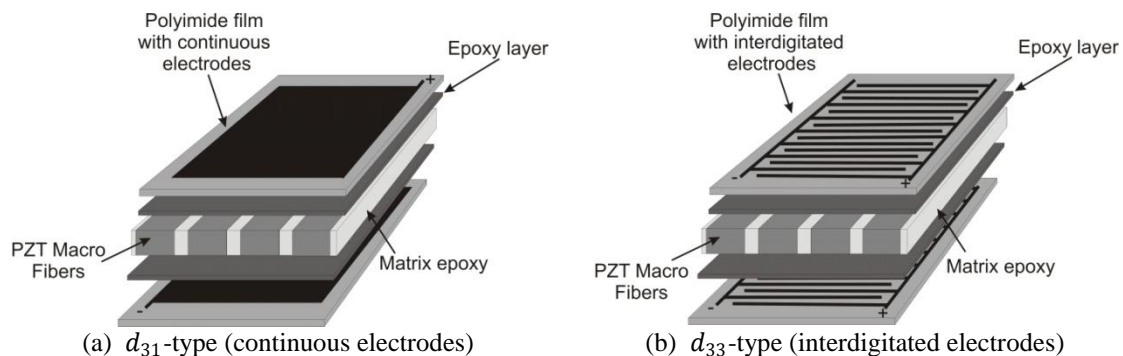


Fig. 6 Typical layout of flat piezocomposite transducers

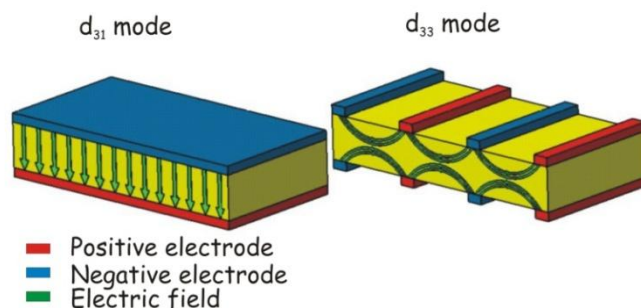


Fig. 7 Electric field distribution for different electrodes configurations

Besides applying prestress to the active layer in order to avoid cracks, these encapsulating layers also bring the electric field to the active layer. The pattern of the electric field depends on the configuration of the electrodes, which can be either continuous (a voltage is applied between the top and the bottom electrodes, resulting in an electric field perpendicular to the plane of the transducer), or interdigitated (positive and negative strip electrodes alternate on each surface of the transducer, resulting in a curved electric field mostly aligned in the direction of the fibers, Hagood 1993). Fig. 7 illustrates the electric fields depending on the electrodes configuration.

In the first case, the piezoelectric fibers are driven in the  $d_{31}$  mode, while in the second case, the fibers are driven in the  $d_{33}$  mode, which allows for a higher achievable free strain but for much higher voltages. Both types of MFCs are currently available on the market, but information found in the datasheets is incomplete and does not contain the full set of piezoelectric properties which are essential for the design of a perfect point load actuator. The limited information found in the datasheet has motivated the study of Deraemaeker *et al.* (Deraemaeker 2009) to derive analytical mixing rules for identifying the equivalent properties of the active layer. These mixing rules linking the material properties to the volume fraction of fibers  $\rho$  in the active layer are summarized in Table 1 for a piezocomposite driven in the  $d_{33}$  mode, where the superscripts  $P, M$  stand for the piezoelectric fiber and epoxy matrix respectively, and the subscripts  $L, T$  stand for longitudinal (in the direction of the fibers) and transverse directions, while the subscript  $z$  represents the out-of-plane direction.

Table 1 Summary of mixing rules for  $d_{33}$ -MFCs (Deraemaeker 2009)

<b>Mechanical properties</b>	
Longitudinal Young's modulus	$E_L = \rho E_L^P + (1 - \rho) E_L^M$
Transverse Young's modulus	$\frac{1}{E_T} = \frac{\rho}{E_T^P} + \frac{1 - \rho}{E_T^M}$
Poisson's ratio	$\nu_{LT} = \rho \nu_{LT}^P + (1 - \rho) \nu_{LT}^M$
Shear modulus	$\frac{1}{G_{LT}} = \frac{\rho}{G_{LT}^P} + \frac{1 - \rho}{G_{LT}^M}$ $G_{Lz} = \rho G_{Lz}^P + (1 - \rho) G_{Lz}^M$ $\frac{1}{G_{Tz}} = \frac{\rho}{G_{Tz}^P} + \frac{1 - \rho}{G_{Tz}^M}$
<b>Piezoelectric properties</b>	
	$d_{33} = \frac{1}{E_L} \rho d_{33}^P E_L^P$ $d_{32} = -d_{33} \nu_{LT} + \rho (d_{32}^P + d_{33}^P \nu_{LT}^P)$
<b>Dielectric properties</b>	
	$\epsilon_{33}^T = \rho \epsilon_{33}^{TP} + (1 - \rho) \epsilon_{33}^{TM}$

Since Eq. (11) involves the  $e_{32}$  and  $e_{31}$  coefficients, it is useful to express these constants as a function of the properties which can be identified from the mixing rules. Under the plane stress hypothesis and for a piezoelectric ceramic poled through the thickness, the  $e_{31}$  and  $e_{32}$  coefficients are linked to the  $d_{31}$  and  $d_{32}$  coefficients through the stiffness matrix  $[c^E]$  as follows (Lee 1990b)

$$\begin{Bmatrix} e_{31} \\ e_{32} \\ e_{36} \end{Bmatrix} = [c^E] \begin{Bmatrix} d_{31} \\ d_{32} \\ d_{36} \end{Bmatrix} = \begin{bmatrix} c_{11}^E & c_{12}^E & 0 \\ c_{12}^E & c_{22}^E & 0 \\ 0 & 0 & c_{66}^E \end{bmatrix} \begin{Bmatrix} d_{31} \\ d_{32} \\ d_{36} \end{Bmatrix} \quad (12)$$

Eq. (12) can be rewritten as a function of the Young's moduli and Poisson's ratios as follows ( $d_{36} = 0$  for a piezoelectric ceramic)

$$e_{31} = \left( \frac{E_L}{1 - \nu_{TL}\nu_{LT}} \right) d_{31} + \left( \frac{\nu_{LT}E_T}{1 - \nu_{TL}\nu_{LT}} \right) d_{32} \quad (13)$$

$$e_{32} = \left( \frac{\nu_{LT}E_L}{1 - \nu_{TL}\nu_{LT}} \right) d_{31} + \left( \frac{E_T}{1 - \nu_{TL}\nu_{LT}} \right) d_{32} \quad (14)$$

The equivalent loads of Eqs. (10) and (11) are derived for a piezoelectric material poled through the thickness ( $d_{31}$ -type MFC). In order to use these expressions for a  $d_{33}$ -type MFC poled through the longitudinal direction, an equivalent model must be defined. Since  $d_{ij}$  corresponds to an expansion in the direction  $j$  for an electric field applied in direction  $i$ , the piezoelectric coefficient  $d_{31}$  of a  $d_{31}$ -type MFC corresponds to the  $d_{33}$  coefficient of a  $d_{33}$ -type MFC. Indeed, directions 1 and 3 in a  $d_{31}$ -type MFC correspond to directions 3 and 1 respectively in a  $d_{33}$ -type MFC, as illustrated in Fig. 8. The same comment can be made for the  $e_{ij}$  coefficients:  $e_{31}$  for a  $d_{31}$ -type MFC corresponds to the  $e_{33}$  coefficient of a  $d_{33}$ -type MFC. In addition, a correction factor of  $h_p/d$ , where  $h_p$  is the thickness of the piezoelectric transducer and  $d$  the spacing between the interdigitated electrodes (Fig. 8), is needed in order to take into account the difference of spacing between the electrodes in the two types of transducers.

This difference results in different values of electric fields for a given applied voltage  $V$  and the correction factor is necessary because the equivalent loads are expressed as a function of  $V$ , assuming that the electric field is equal to  $E_3 = -V/h_p$ . For the application of Eqs. (10) and (11), the correction factor must be applied to both  $e_{31}$  and  $e_{32}$ . For MFCs, the value of  $h_p/d$  is 0.36 (Deraemaeker 2009).

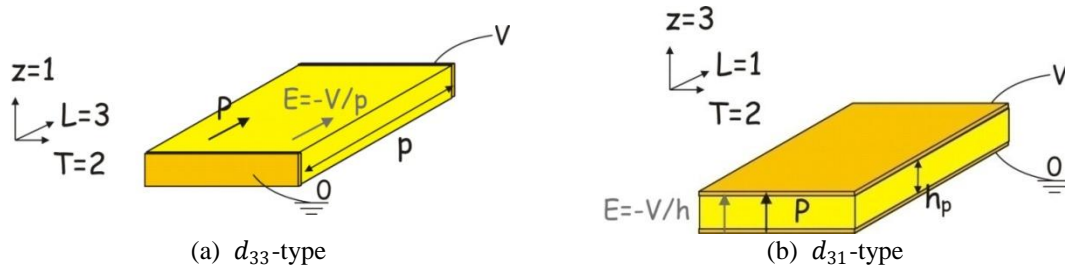
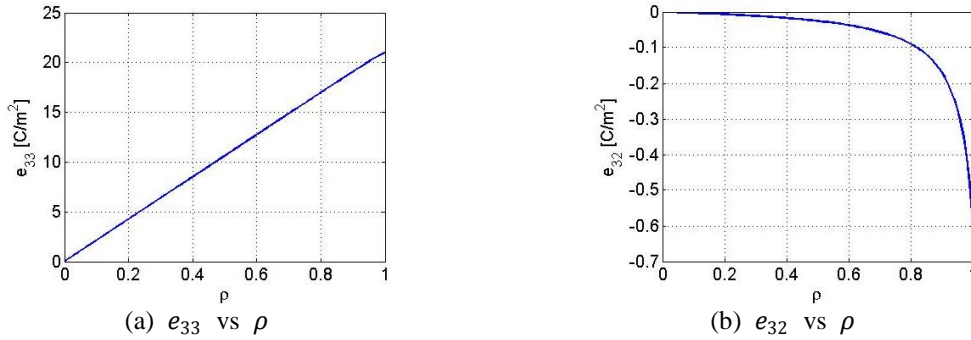


Fig. 8 Equivalences of the 1-3 directions for  $d_{33}$ -type and  $d_{31}$ -type MFCs

Table 2 Physical properties of the piezocomposite constitutive materials

$d_{33}$ MFC Homogenized properties	Unit	Epoxy	SONOX P502
Young's modulus	GPa	$E_L^M = 2.9$	$E_L^P = 48.3$
	GPa	$E_T^M = 2.9$	$E_T^P = 54.05$
Shear modulus	GPa	$G_{LT}^M = 1.885$	$G_{LT}^P = 19.48$
Poisson's ratio	-	$\nu_{LT}^M = 0.3$	$\nu_{LT}^P = 0.4$
Mass density	kg/m <sup>3</sup>	1000	7800
Piezoelectric charge constants	pC/N	/	$d_{32} = -185$
	pC/N	/	$d_{33} = 440$
Dielectric relative constant	-	$\epsilon_{33}^{T,M}/\epsilon_0 = 4.25$	$\epsilon_{33}^{T,P}/\epsilon_0 = 1850$

Fig. 9 Evolution of piezoelectric constants with respect to the volume fraction of fibers  $\rho$  for a  $d_{33}$ -type MFC

### 3.3 Design of a perfect point load actuator

Consider a  $d_{33}$ -type MFC with its active layer made of epoxy and SONOX P502 fibers with properties summarized in Table 2.

Using the mixing rules of Table 1, the evolution of the piezoelectric constants  $e_{33}$  and  $e_{32}$  with respect to the volume fraction of fibers  $\rho$  can be plotted, and is shown in Fig. 9.

We see from Fig. 9 the interest of considering piezocomposite transducers with interdigitated electrodes:  $e_{33}$  and  $e_{32}$  evolve with opposite signs, allowing to satisfy Eq. (10), and providing therefore a possibility to achieve a perfect point load actuator. The evolution of the ratio  $b/l$  for a 1 mm thick triangular  $d_{33}$ -type MFC as a function of the volume fraction of fibers  $\rho$  based on Eq. (10), where  $e_{31}$  has been replaced by  $e_{33}$ , as well as the point force at the tip of the triangle for a unitary voltage (Eq. (11)) as a function of  $\rho$ , are plotted in Fig. 10 ( $z_m = 0.65$  mm), taking into account the correction factor  $h_p/d=0.36$ .

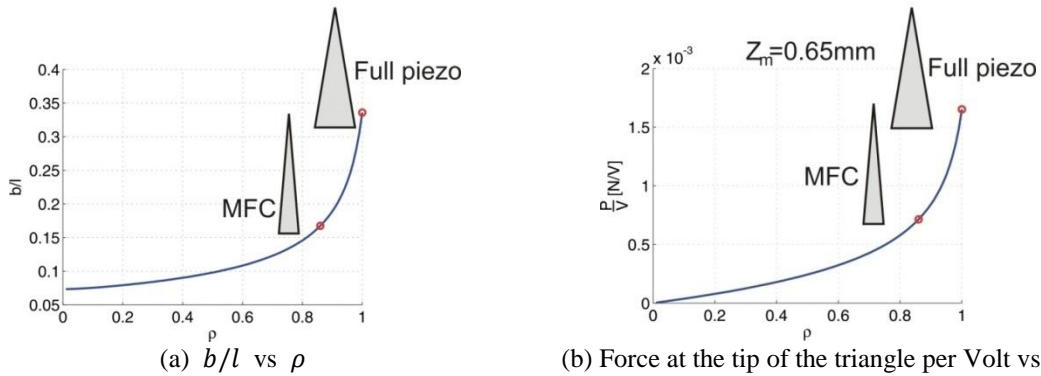


Fig. 10 Evolution of the geometry and the force of a perfect point load actuator as a function of the volume fraction of fibers  $\rho$  for a  $d_{33}$ -type MFC

It is obvious from Fig. 10 that a full piezoelectric transducer ( $\rho = 1$ ) produces the highest force. However, with such a configuration, the transducer presents the drawbacks of the PZT ceramics which are their brittleness and very low flexibility, making this solution difficult to implement (the use of an epoxy package can improve the flexibility of such actuators for a mounting on slightly curved structures). For practical reasons, it is therefore preferable to consider piezocomposites for which the volume fraction of fibers  $\rho$  is a trade-off between the amplitude of the force to be applied, and the flexibility needed. As an example, a typical  $d_{33}$ -type MFC from *Smart Material* ( $\rho = 86\%$ ) can be used for the design of a point load actuator by shaping the electrodes with a triangle of aspect ratio  $b/l = 0.167$ , which leads to a point-force of  $0.00072\text{N/V}$ .

Fig. 11 gives a schematic view of the practical implementation of a perfect point load actuator based on a  $d_{33}$ -type MFC with interdigitated electrodes:

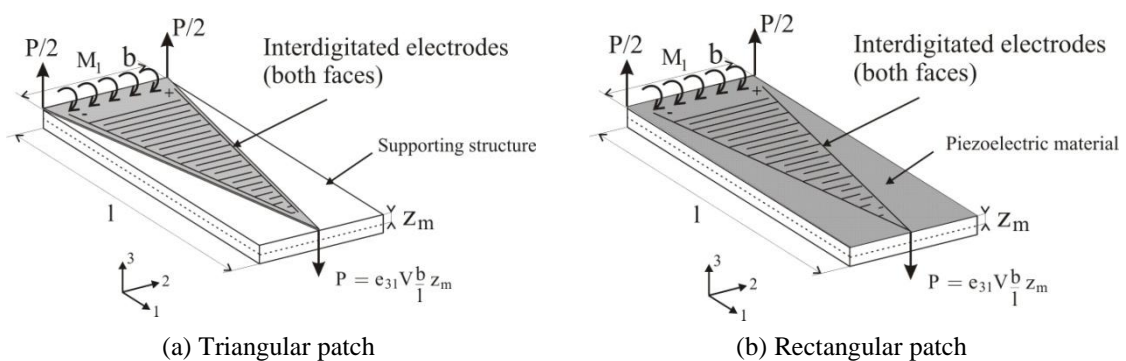


Fig. 11 Practical implementation of the perfect point load actuator based on a  $d_{33}$ -type MFC with interdigitated electrodes

Since the loads applied by the piezoelectric transducer depend only on the shape of the electrodes, a perfect point load actuator based on a  $d_{33}$ -type MFC should have interdigitated electrodes shaped as a triangle on both top and bottom surfaces. The piezocomposite material can be either shaped as a triangle (Fig. 11(a)) or as rectangle (Fig. 11(b)), since only the shape of the electrodes defines the loads applied by the actuator.

#### 4. Finite element verification

In order to validate the design of a perfect point load actuator based on a  $d_{33}$ -type MFC, we investigate a problem similar to the one studied experimentally by Gardonio *et al.* in (Gardonio 2010). It consists in a  $414\text{ mm} \times 314\text{ mm} \times 1\text{ mm}$  aluminum plate clamped on its edges, on which a triangular piezoelectric transducer is fixed on the top surface in order to produce a point load, as illustrated in Fig. 12. The computations are performed using multi-layer piezoelectric plate elements available in the finite element package *SAMCEF*. The structure is discretized with 8761 elements, leading to 27145 degrees of freedom (27144 mechanical degrees of freedom and one electrical degree of freedom).

Table 3 Homogenized properties of the active layer of  $d_{33}$ -type MFC calculated using the analytical mixing rules of Table 1

$d_{33}$ MFC Homogenized properties	Symbol	Unit	Mixing rules ( $\rho = 1$ )	Mixing rules ( $\rho = 0.86$ )
Young's modulus	$E_L$	GPa	48.30	41.94
	$E_T$	GPa	54.05	15.58
Shear modulus	$G_{LT}$	GPa	19.48	8.44
Poisson's ratio	$\nu_{LT}$	-	0.4	0.38
Mass density	$\rho_m$	kg/m <sup>3</sup>	7800	6848
Piezoelectric charge constants	$d_{32}$	pC/N	-185	-175.86
	$d_{33}$	pC/N	440	435.74
Dielectric relative constant	$\epsilon_{33}^T/\epsilon_0$	-	1850	1591

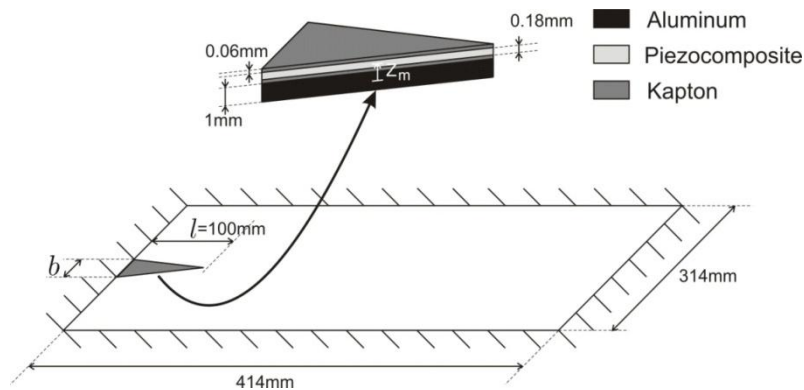


Fig. 12 Description of the numerical case study

The performance of a point load  $d_{33}$ -type MFC with interdigitated electrodes is assessed for two volume fractions of SONOX P502 fibers (from *CeramTec*): (i) active layer consisting in a full piezoelectric patch ( $\rho = 1$  leading to a ratio  $b/l = 0.336$ ), and (ii) a typical volume fraction of the commercially available  $d_{33}$ -type MFC actuator from *Smart Material* ( $\rho = 0.86$  leading to a ratio  $b/l = 0.167$ ). The homogenized properties of the active layer obtained by applying the mixing rules of Table 1 are summarized in Table 3.

In order to evaluate the performance of such transducers, the results are compared to (i) a real point load applied to the tip of the triangle, and (ii) the results obtained with a triangular patch with an aspect ratio  $b/l = 0.336$  but with an active layer made of an isotropic piezoelectric patch (SONOX P502) poled through the thickness, similar to the design in (Gardonio 2010). The later is referred to as  $d_{31}$ -type actuator and does not lead to perfect point load actuation since Eq. (10) is not satisfied, resulting in applied bending moments along the edges of the triangle.

The static deflections of the plate due to a unitary voltage for a  $d_{33}$ -type MFC actuator ( $\rho = 1$  and  $b/l = 0.336$ ) with interdigitated electrodes and a  $d_{31}$ -type actuator with continuous electrodes are illustrated in Fig. 13 to Fig. 15.

A quantitative comparison of the deflection projected on each component of the displacement and rotation fields can be given by computing the MAC (Modal Assurance Criterion, Ewins 1984) value between the deflection due to unitary voltage  $\varphi_V$  and the deflection due to a point load  $\varphi_P$ . The MAC is defined by

$$MAC = \frac{\varphi_V^T \varphi_P}{(\varphi_V^T \varphi_V)(\varphi_P^T \varphi_P)} \tag{15}$$

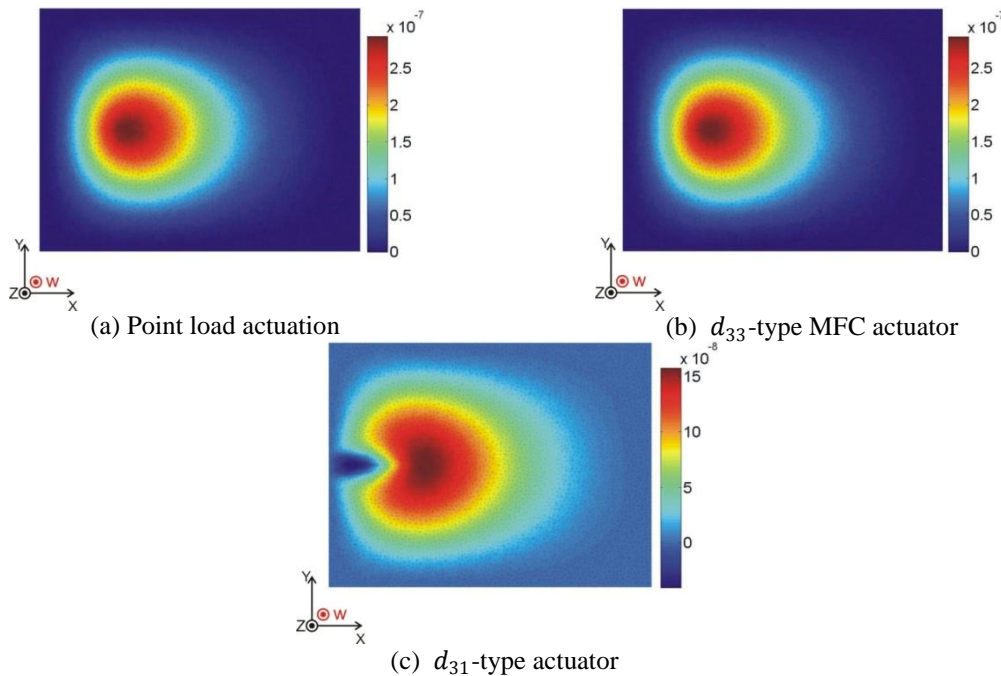


Fig. 13 Static deflection ( $w$ : displacements along  $z$ ) under unitary voltage

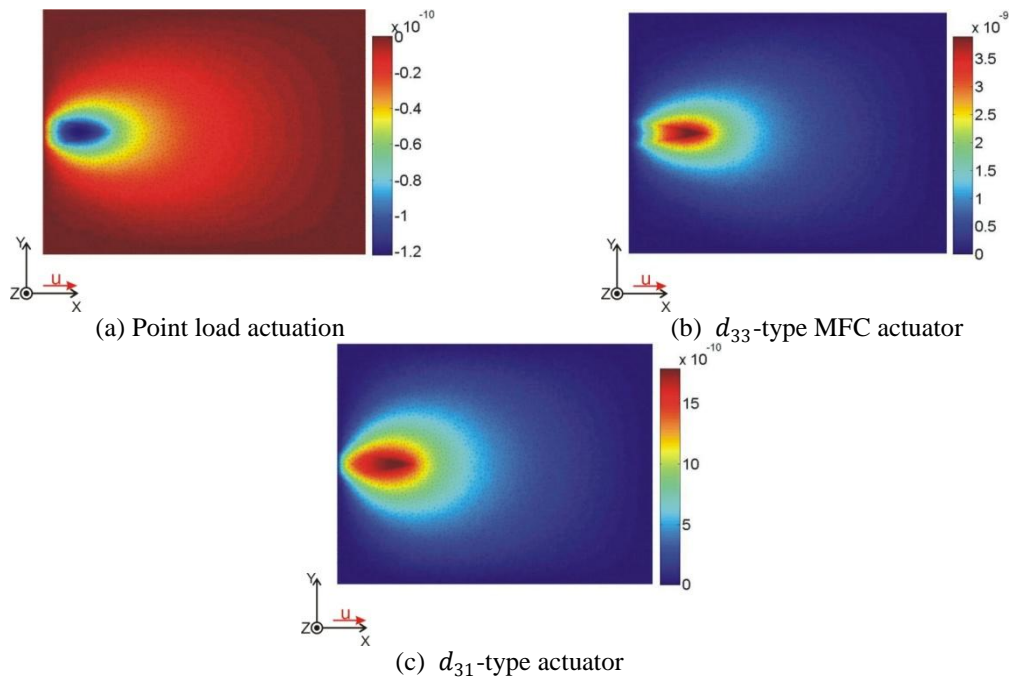


Fig. 14 Static deflection ( $u$ : displacements along  $x$ ) under unitary voltage

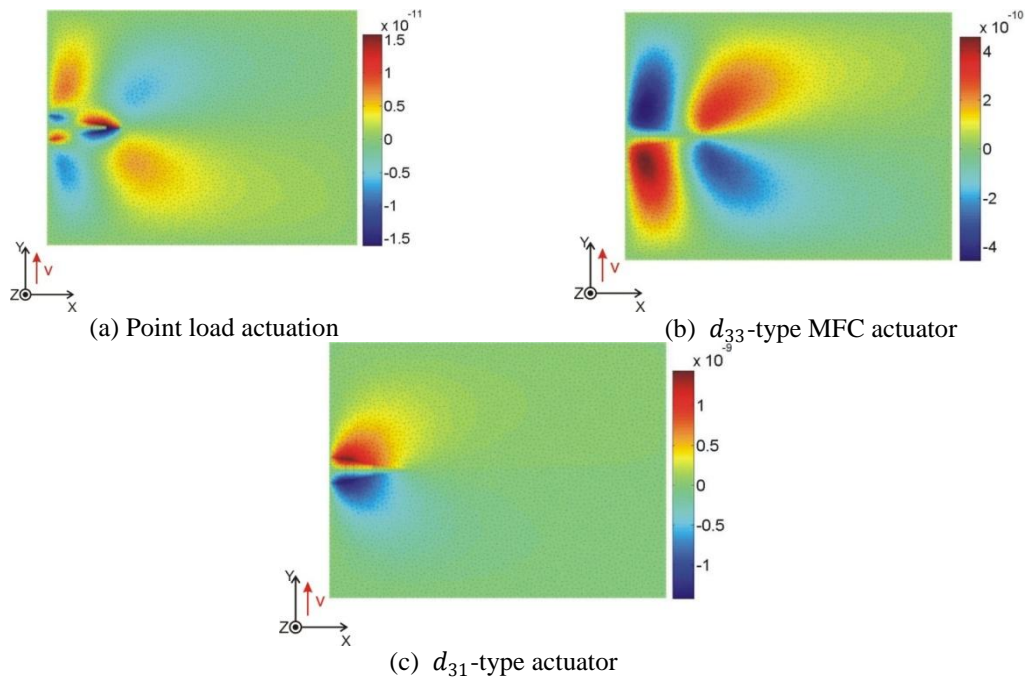


Fig. 15 Static deflection ( $v$ : displacements along  $y$ ) under unitary voltage

Table 4 MAC values between the static deformation under unitary point load and unitary voltage

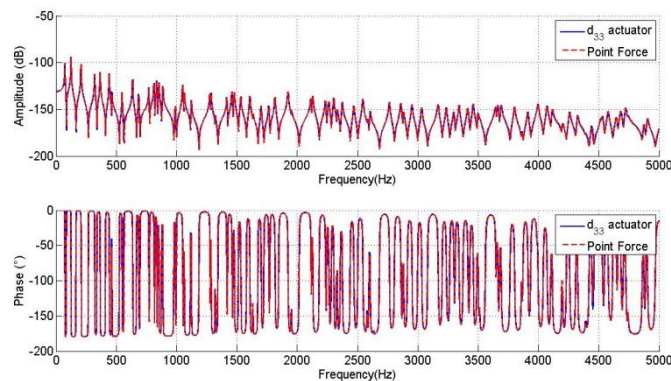
	$d_{33}$ -type	$d_{31}$ -type
$u$	1	1
$v$	0.6418	0.2061
$w$	1	0.9655
$\theta_x$	1	0.4447
$\theta_y$	1	0.8309

Table 5 Maximum amplitude for each component of the displacement and rotation fields

	Point load	$d_{33}$ -type	$d_{31}$ -type
$u$ (m)	$1.2189 \cdot 10^{-10}$	$3.8900 \cdot 10^{-9}$	$1.7843 \cdot 10^{-9}$
$v$ (m)	$1.6056 \cdot 10^{-11}$	$4.5673 \cdot 10^{-10}$	$1.4264 \cdot 10^{-9}$
$w$ (m)	$2.9282 \cdot 10^{-7}$	$2.9155 \cdot 10^{-7}$	$1.5719 \cdot 10^{-7}$
$\theta_x$ (rad)	$2.6834 \cdot 10^{-6}$	$2.6731 \cdot 10^{-6}$	$6.1910 \cdot 10^{-6}$
$\theta_y$ (rad)	$3.8428 \cdot 10^{-6}$	$3.8731 \cdot 10^{-6}$	$3.5244 \cdot 10^{-6}$

Table 4 summarizes the MAC values as well as the maximum amplitude for each type of actuator, while Table 5 provides the maximum deflection in each direction.

For the  $d_{33}$ -type MFC actuator, Tables 4 and 5 as well as Fig. 13 to 15 show an excellent match for the rotations ( $\theta_x$ ,  $\theta_y$ ) and for  $w$ . There are noticeable differences for the in-plane displacement  $u$  and  $v$ . For the point load actuation,  $u$  and  $v$  are non-zero due to the non-symmetric layout of the plate with respect to the neutral plane in the region of the triangular actuator (membrane-bending coupling). For the  $d_{33}$ -type MFC actuator, additional in-plane displacements are due to the in-plane forces generated at the edges of the actuator, causing higher amplitudes of in-plane displacement. Such in-plane forces have not been derived in this study. The resulting deflections are however several orders of magnitude lower than in the  $z$ -direction. Although they might be important to consider if a piezoelectric patch is used as a sensor collocated to the actuator on the opposite side of the supporting plate, they can in general be considered as negligible.

Fig. 16 Comparison of the FRFs for a point load and a  $d_{33}$  full piezo actuator ( $\rho = 1$ )

For the  $d_{31}$ -type actuators, the match is not very good, showing, as expected, that such a solution is not suitable to achieve point load actuation.

Since one of the interests of a perfect point load actuator lies in the active damping of structures by using a collocated sensor-actuator pair, we compare the frequency response function (FRF) between the vertical displacement  $w$  at the tip of the triangular actuator and (i) a vertical perfect point load applied at the same position or (ii) the voltage applied between the electrodes of the triangular piezocomposite when it is used as an actuator.

Figures 16 and 17 show that for both designs of  $d_{33}$ -MFC actuator, the FRFs corresponding to a point load actuation and a piezoelectric actuation are identical. Figure 18 shows the comparison of the FRF between the vertical displacement at the tip of the triangular  $d_{33}$ -MFC actuator and the voltage applied for  $\rho = 0.86$  and  $\rho = 1$ .

The frequency response corresponding to a full piezoelectric actuator is globally\* the frequency response corresponding to a volume fraction of fibers of  $\rho = 0.86$  shifted of 7.28dB (Fig. 18). It could be expected from Fig. 10(b), which shows that a full piezoelectric actuator applies a force 2.3132 times bigger than an actuator with a volume fraction of fibers of  $\rho = 0.86$ .

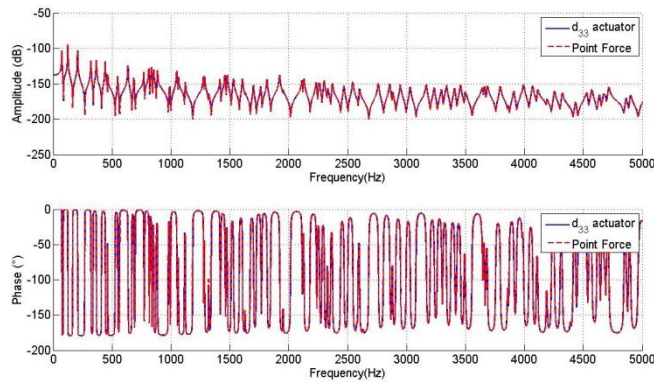


Fig. 17 Comparison of the FRFs for a point load and a  $d_{33}$  MFC actuator ( $\rho = 0.86$ )

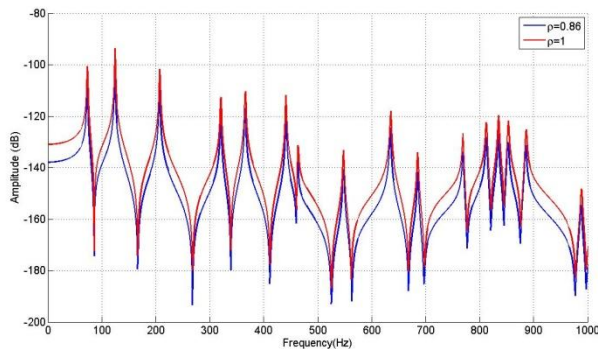


Fig. 18 Comparison of the FRFs for a point load and a  $d_{33}$  MFC actuator ( $\rho = 0.86$  and  $\rho = 1$ )

\* Because the change of the shape of the actuator changes slightly the global structure, the frequency response for  $\rho = 1$  is not exactly the frequency response for  $\rho = 0.86$  shifted of 7.28dB.

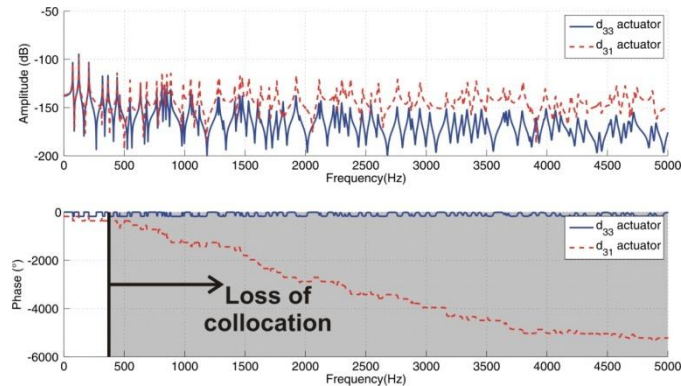


Fig. 19 Comparison of the FRFs for a  $d_{33}$  full piezo actuator ( $\rho = 1$ ) with interdigitated electrodes and a  $d_{31}$ -type actuator with continuous electrodes

By following the design rules detailed in Section 3.3, we can see that a  $d_{33}$ -type actuator with interdigitated electrodes is able to behave like a perfect point load actuator. On the other hand, an isotropic  $d_{31}$ -type actuator with continuous electrodes is not able to act as a point load actuator (Fig. 19). In particular, the collocation (phase varying between  $0^\circ$  and  $\pm 180^\circ$ ) is lost at a very low frequency (around 400Hz), which reduces drastically the frequency band in which such a transducer can be used for collocated active damping of structures via velocity feedback control. Indeed, it is well-known (Preumont 2002) that the open-loop FRF of a sensor collocated with an actuator should have alternating poles and zeros (leading to a phase varying between  $0^\circ$  and  $\pm 180^\circ$ ) in order to guarantee the stability of the velocity feedback loop.

## 5. Conclusions

In this paper, we investigated the conditions required to design a perfect point load actuator based on triangular flat piezoelectric patches. The equivalent loads applied by a triangular flat piezoelectric actuator clamped on one of its edges on the host plate structure consist in a point load at the free tip as well as distributed moments along the two free edges of the triangular electrodes. Based on the expression of these distributed moments, we have derived the condition to cancel them. This condition relates the shape ( $b/l$  ratio) of the triangle to the ratio of its in-plane piezoelectric properties ( $e_{31}/e_{32}$ ) and can only be met if the later ratio is negative, calling for a design with interdigitated electrodes rather than continuous ones. In addition, we have discussed the possibility to vary the  $e_{31}/e_{32}$  ratio by using piezocomposite transducers with different volume fractions of piezoelectric fibers, resulting in a different shape of the triangle and a different magnitude of the point load. These results show that the choice of the shape of the triangle (and therefore the volume fraction of PZT fibers) is fixed by a trade-off between the amplitude of the force needed (which is maximum for a full ceramic patch), and the flexibility needed by the actuator to be attached to curved structures. The design has been validated numerically on a plate clamped on all its edges to which different triangular piezoelectric patches have been attached: two piezocomposite actuators with interdigitated electrodes (full ceramic patch and a typical MFC actuator from *Smart Material* with a volume fraction of SONOX P502 fibers of 86%) and one

isotropic piezoelectric patch with continuous electrodes. It has been demonstrated that the static deflections under point load and under actuation with a piezocomposite with interdigitated electrodes are in perfect agreement. Moreover, the frequency responses between the vertical displacement at the tip of the triangle and the point load or the voltage applied between the electrodes of the piezocomposite are also matching perfectly. On the other hand, the static deflection due to an isotropic actuator shows clearly that there are only distributed moments along the edges of the electrodes, with no point force. As a result, the collocation is lost at a very low frequency so that such piezoelectric transducers are not suited for velocity feedback damping. Future work will focus on the robustness of the design with respect to uncertainties in the material properties and in the geometry of the electrodes of the actuator before experimental validation.

## References

- Burke, S.E. and Hubbard, J.E. (1987), "Active vibration control of a simply supported beam using a spatially distributed actuator", *IEEE Contr. Syst. Mag.*, **7**(4), 25-30.
- Carbonari, R.C., Silva, E.C.N. and Paulino, G.H. (2009), "Multi-actuated functionally graded piezoelectric micro-tools design: a multiphysics topology optimization approach", *Int. J. Numerical Meth. Eng.*, **77**(3), 301-336.
- Chesné, S., Chomette, B. and Pezerat, C. (2008), "Measurements of the bending moment at boundaries of a structure", *Proceedings of the Acoustics 08*, Paris, France.
- Deraemaeker, A., Nasser, H., Benjeddou, A. and Preumont, A. (2009), "Mixing rules for the piezoelectric properties of Macro Fiber Composites", *J. Intell. Mater. Syst. Struct.*, **20**(12), 1475-1482.
- Deraemaeker, A., Tondreau, G. and Bourgeois, F. (2011), "Equivalent loads for two-dimensional distributed anisotropic piezoelectric transducers with arbitrary shapes attached to thin plate structures", *J. Acoust. Soc. Am.*, **129**(2), 681-690.
- Donoso, A. and Bellido, J.C. (2009), "Tailoring distributed modal sensors for in-plane modal filtering", *Smart Mater. Struct.*, **18**(3), 1-4.
- Ewins, D.J. (1984), *Modal testing: theory and practice*, Research Studies Press LTD, Letchworth.
- Friswell, M.I. and Adhikari, S. (2010a), "Sensor shape design for piezoelectric cantilever beams to harvest vibration energy", *J. Appl. Phys.*, **108**(1), 014901, 1-6.
- Friswell, M.I. and Adhikari, S. (2010b), "Structural health monitoring using shaped sensors", *Mech. Syst. Signal Pr.*, **24**(3), 623-635.
- Gardonio, P. and Elliott, S.J. (2005), "Smart panels with velocity feedback control systems using triangularly shaped strain actuators", *J. Acoust. Soc. Am.*, **117**(4), 2046-2064.
- Gardonio, P., Aoki, Y. and Elliott, S.J. (2010), "A smart panel with active damping wedges along the perimeter", *Smart Mater. Struct.*, **19**(6), 1-15.
- Hagood, N., Kindel, R., Ghandi, K. and Gaudenzi, P. (1993), "Improving transverse actuation of piezoceramics using interdigitated surface electrodes", *Proceedings of the SPIE 1917*, Albuquerque, USA.
- Isarakorn, D., Briand, D., Sambri, A., Gariglio, S., Triscone, J.M., Guy, F., Reiner, J.W., Ahn, C.H. and de Rooij, N.F. (2011), "Finite elements analysis and experiments on a silicon membrane actuated by an epitaxial PZT film for localized-mass sensing applications", *Sensor. Actuat. B – Chem.*, **153**(1), 54-63.
- Lee, C.K. and Moon, F.C. (1990a), "Modal sensors/actuators", *J. Appl. Mech.- TASEM*, **57** (2), 434-441.
- Lee, C.K. (1990b), "Theory of laminated piezoelectric plates for the design of distributed sensors/actuators, part I: governing equations and reciprocal relationships", *J. Acoust. Soc. Am.*, **87**(3), 1144-1158.
- Lee, C.K., Chiang, W.W. and O'Sullivan, T.C. (1991), "Piezoelectric modal actuator/sensor pairs for critical active damping vibration control", *J. Acoust. Soc. Am.*, **90**(1), 374-384.

- Lin, Z. and Wang, X. (2013), "Development of functionally graded flextensional piezoelectric devices designed by topology optimization", *Proceedings of the WCSMO-10*, Orlando, USA.
- Newnham, R.E., Bowen, L.J., Klicker, K.A. and Cross, L.E. (1980), "Composite piezoelectric transducers", *Mater. Design*, **2**(2), 93-106.
- Park, G., Sohn, H., Farrar, C.R. and Inman, D.J. (2003), "Overview of piezoelectric impedance-based health monitoring and path forward", *Shock Vib. Digest*, **35**(6), 451-463.
- Paulitsch, C., Gardonio, P. and Elliott, S.J. (2007), "Active vibration damping using an inertial electrodynamic actuator", *J. Vib. Acoust.*, **129**(1), 39-47.
- Preumont, A. (2002), *Vibration control of active structures, an introduction*, Kluwer Academic Publishers, Dordrecht.
- Preumont, A., de Marneffe, B., Deraemaeker, A. and Bossens, F. (2008), "The damping of a truss structure with a piezoelectric transducer", *Comput. Struct.*, **86**(3-5), 227-239.
- Raghavan, A. and Cesnik, C.E.S. (2007), "Review of guided-wave structural health monitoring", *J. Vib. Acoust.*, **39**(2), 91-114.
- Raman, S.R., Tondreau, G. and Deraemaeker, A. (2012), "Design of a point load actuator based on a triangular piezoelectric patch", *Proceedings of the EACS2012*, Genoa, Italy.
- Schiller, N.H., Cabell, R.H. and Fuller, C.R. (2008), "Decentralized control of sound radiation using a high authority/low-authority control strategy with anisotropic actuators", *Proceedings of the Acoustics 08*, Paris, France.
- Sullivan, J.M., Hubbard, J.E. and Burke, S.E. (1996), "Modelling approach for two-dimensional distributed transducers of arbitrary spatial distribution", *J. Acoust. Soc. Am.*, **99**, 2965-2974.
- Sullivan, J.M., Hubbard, J.E. and Burke, S.E. (1997) "Distributed sensor/actuator design for plates: spatial shape and shading as design parameters", *J. Sound Vib.*, **203**, 473-493.
- Williams, B., Park, G., Inman, D. and Wilkie, W. (2002), "An overview of composite actuators with piezoceramic fibers", *Proceedings of the IMACXX*, Los Angeles, USA.